NANO LETTERS

pubs.acs.org/NanoLett Letter

Predictive High-Throughput Platform for Dual Screening of mRNA Lipid Nanoparticle Blood–Brain Barrier Transfection and Crossing

Emily L. Han, Marshall S. Padilla, Rohan Palanki, Dongyoon Kim, Kaitlin Mrksich, Jacqueline J. Li, Sophia Tang, Il-Chul Yoon, and Michael J. Mitchell*

Cite This: https://doi.org/10.1021/acs.nanolett.3c03509 Read Online

ACCESS | Metrics & More | Article Recommendations | Supporting Information

ABSTRACT: Lipid nanoparticle (LNP)-mediated nucleic acid therapies, including mRNA protein replacement and gene editing therapies, hold great potential in treating neurological disorders including neurodegeneration, brain cancer, and stroke. However, delivering LNPs across the blood–brain barrier (BBB) after systemic administration remains underexplored. In this work, we engineered a high-throughput screening transwell platform for the BBB (HTS-BBB), specifically optimized for screening mRNA LNPs. Unlike most transwell assays, which only assess transport across an endothelial monolayer, HTS-BBB simultaneously measures LNP transport and mRNA transfection of the endothelial cells themselves. We then use HTS-BBB to screen a library of 14 LNPs made with structurally diverse ionizable lipids and demonstrate it is predictive of *in vivo* performance by validating lead candidates for mRNA delivery to the mouse brain after intravenous injection. Going forward, this platform could be used to screen large libraries of brain-targeted LNPs for a range of protein replacement and gene editing applications.

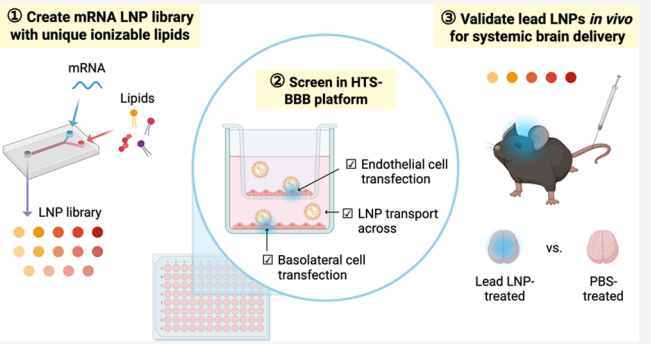

KEYWORDS: *lipid nanoparticle, mRNA, brain delivery, blood–brain barrier*

Neurological disorders are the leading cause of disability and second leading cause of death globally.[1] Among the leading causes of death are stroke and dementias, including Alzheimer's disease.[1] Over the past few decades, nucleic acid therapeutics such as messenger RNA (mRNA) for protein replacement or gene editing therapy and small interfering RNA (siRNA) have begun to be explored for treating neurological disorders.[2,3] Recent examples from literature include heme oxygenase 1 self-replicating mRNA to treat stroke,[4] brain-derived neurotrophic factor mRNA and beta-secretase 1 siRNA to treat Alzheimer's disease,[5−11] synuclein alpha siRNA to treat Parkinson's disease,[12,13] tumor necrosis factor-related apoptosis-inducing ligand mRNA and CD47 and PD-L1 siRNA among others to treat glioblastoma,[14−16] Cas9 mRNA and single guide RNA targeting PLK1 to treat glioblastoma,[17] and base editing mRNA with single guide RNA to treat congenital brain disease.[18]

Ionizable lipid nanoparticles (LNPs) are an ideal delivery vehicle for nucleic acid therapeutics.[19] LNPs have achieved recent success in the clinic, including the FDA approval of Onpattro, an LNP formulation delivering siRNA for hereditary transthyretin-mediated amyloidosis, and the Pfizer-BioNTech and Moderna COVID-19 mRNA vaccines.[20] LNPs are typically composed of four lipid components: an ionizable lipid for loading and facilitating endosomal escape of nucleic acid cargo, a phospholipid for structural stability, cholesterol for rigidity, and a lipid-polyethylene glycol (PEG) for reducing aggregation.[21] LNPs have several key advantages over traditional viral vectors, including having excellent biocompatibility allowing for repeat dosing, no risk for genomic integration, and no strict transgene size limitations.[18,22] Furthermore, the highly modular nature of LNPs allows them to be optimized for organ- and cell type-specific delivery following systemic administration.[23−25]

Achieving LNP delivery to the brain via systemic administration would be highly desirable. Systemic administration routes like intravenous injection hold many benefits over direct brain and cerebrospinal fluid injections, which are limited by being highly invasive, technically complex, and having limited diffusion from the injection site.[2,26] However, LNP delivery to the brain via systemic administration remains underexplored.[27] The blood–brain barrier (BBB), composed of cellular components including endothelial cells, capillary

Received: September 13, 2023
Revised: December 19, 2023
Accepted: December 20, 2023

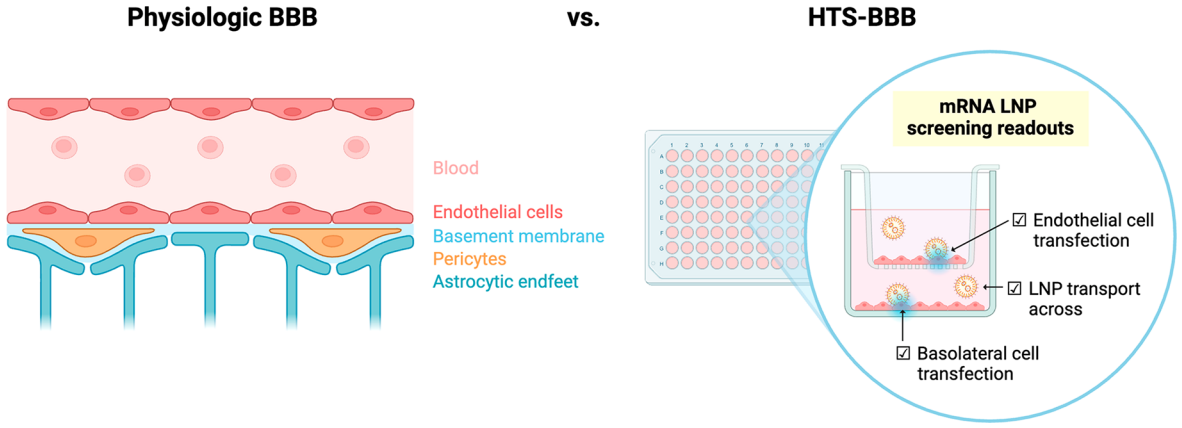

Figure 1. Schematic of blood–brain barrier (BBB) physiology and the development of the high-throughput screening BBB (HTS-BBB) platform for identifying mRNA lipid nanoparticles (mRNA LNPs) that cross the BBB and also transfect the BBB for neurological disorder applications.

basement membrane, astrocytes, and pericytes, prevents approximately 98% of small molecule drugs and approximately 100% of large molecule drugs from entering the brain.[28] LNPs must also cross this highly selective barrier in order to reach the brain. Recent advances in the field include those by Ma et al., who designed LNPs with tryptamine-inspired lipids that facilitated the delivery of the small molecule drug amphotericin B, antisense oligonucleotides (ASOs), and gene editing Cre protein across the BBB. However, as only 0.1% of the injected amphotericin B was delivered to the brain, the delivery efficiency remains low.[29]

One of the rate-limiting factors in designing LNPs with higher brain delivery efficiency after systemic administration is the lack of informative *in vitro* screening platforms. Brain endothelial monolayers grown in traditional 96-well plates can screen for transfection in a high-throughput manner, but the lack of two compartments means that they cannot measure transport across the BBB.[30] BBB transwell models have a semipermeable membrane separating two compartments allowing for transport measurements but are low-throughput as they are typically only used in 12- or 24-well formats and do not capture transfection.[30,31] An ideal *in vitro* screening system would screen for both endothelial transfection and transport. Top candidates for endothelial transfection could be used for applications such as repairing the BBB after injury or during disease,[32,33] as demonstrated by Marcos-Contreras et al. delivering thrombomodulin mRNA LNPs to the brain endothelium in mice with acute brain inflammation.[34] Top candidates for transport across the BBB could be optimized to target other brain cell types of interest, such as neurons.

Here, we develop a BBB transwell model for high-throughput screening of mRNA LNPs (HTS-BBB), built in a 96-well plate format, for simultaneous measurement of transfection of the brain endothelial monolayer as well as transport across the monolayer (Figure 1). Additionally, by being able to screen large libraries of LNPs on a single plate rather than across multiple 12- or 24-well transwell plates, we can achieve more consistent results, save material costs by requiring less cells and media, and increase workflow speed by using multichannel pipettes and potentially automated robotic handling in the future. We first optimize HTS-BBB monolayer growth conditions, as well as mRNA reporters for transfection and fluorescent dye reporters for transport. We then screen a library of 14 LNPs with unique ionizable lipid structures, and examine correlations between transport and transfection, LNP size, and LNP zeta potential. Finally, we demonstrate that HTS-BBB is predictive of *in vivo* performance by validating lead candidates for delivery of mRNA to the mouse brain following intravenous injection.

OPTIMIZING BRAIN ENDOTHELIAL MONOLAYER GROWTH IN HTS-BBB

In order to develop a high-throughput platform to screen mRNA LNPs for transfection of and transport across the BBB, we created HTS-BBB on a 96-well transwell plate. Each well consists of a brain endothelial monolayer grown on a semipermeable membrane separating the apical compartment, representing the blood side, and the basolateral compartment, representing the brain side. In order to accurately assess LNP transport across the brain endothelial monolayer, the monolayer must not have any gaps or overgrowth. Thus, we began by optimizing the monolayer growth conditions (Figure 2A). Immortalized human microvascular brain endothelial (hCMEC/D3) cells were chosen as the cell line as they (i) are able to form contact-inhibited monolayers when grown on collagen type 1, a key component of the BBB basement membrane, and (ii) express tight and adherens junctions, which help regulate the structural integrity and permeability of the BBB.[35,36]

hCMEC/D3 cells were seeded at 20,000, 30,000, and 40,000 cells/cm^2 on the 96-well transwell inserts, and their growth was monitored daily via live/dead imaging (Figure S1). A complete monolayer without overgrowth was formed at Day 6 after initial cell seeding with an initial seeding density of 30,000 cells/cm^2 (Figure 2B). In comparison, shorter growth time and lower seeding densities resulted in an incomplete monolayer, while longer growth time and higher seeding densities resulted in overconfluence of cells. To confirm the presence of a monolayer, we analyzed the orthogonal view of Z-stacked images acquired via confocal microscopy (Figure S2). Moreover, the optimized monolayer strongly expressed ZO-1 and VE-cadherin, proteins which contribute to tight and adherens junction integrity (Figure 2C).[36]

Next, we assessed the functional integrity of the brain endothelial monolayer by monitoring the transport of 10 and 70 kDa of FITC-dextran (FD) across the monolayer. On Day 6 after the initial seeding of cells on the transwell membrane, the 10 kDa FD displayed low transport values of around 5%, and the 70 kDa FD displayed even lower transport at around 2%, which we expected given its higher molecular weight (Figure

https://doi.org/10.1021/acs.nanolett.3c03509
Nano Lett. XXXX, XXX, XXX−XXX

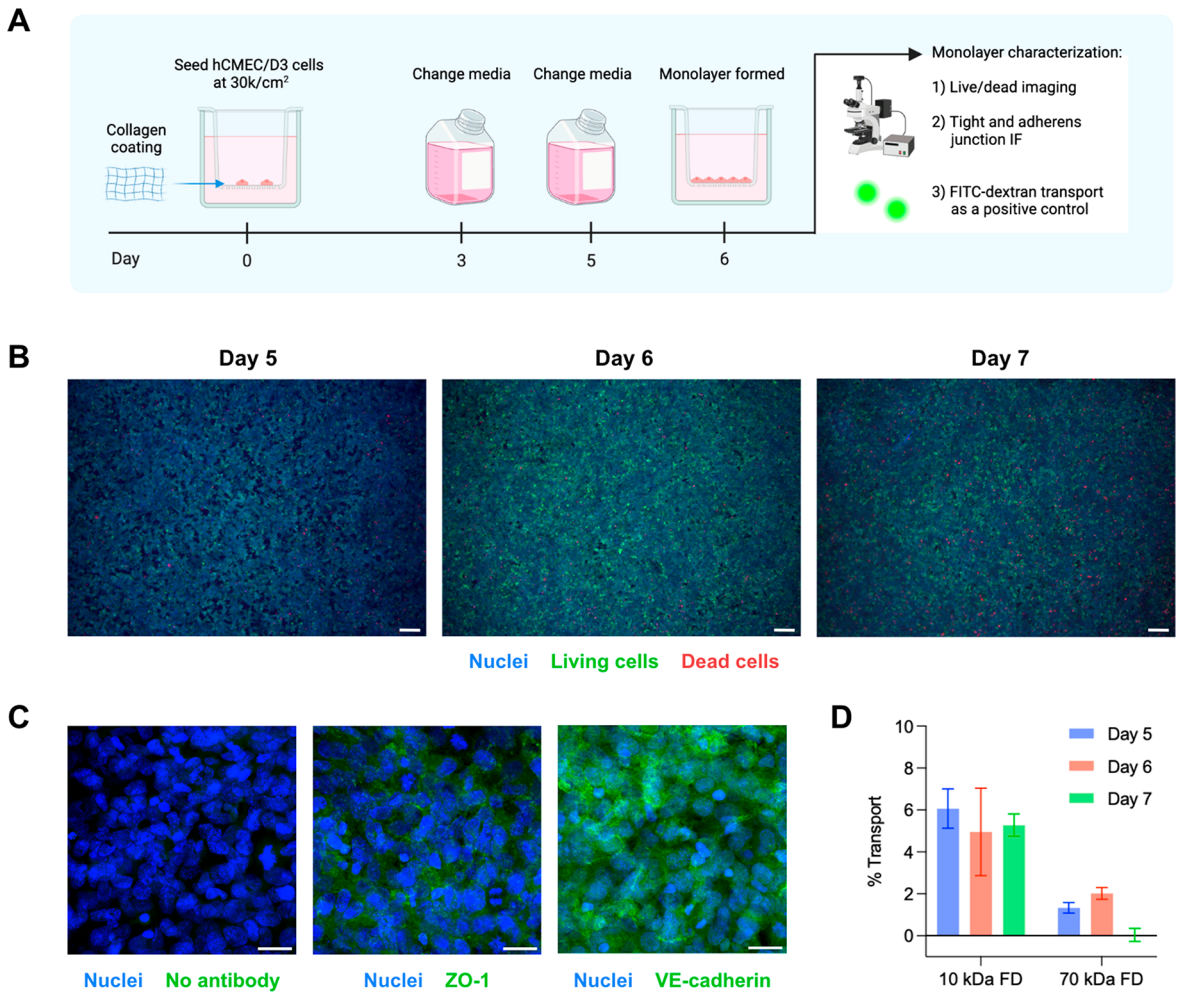

Figure 2. Optimization of brain endothelial monolayer growth in HTS-BBB. A) Schematic showing endothelial monolayer growth timeline and characterization techniques. B) Live/dead imaging of a monolayer seeded at 30,000 cells/cm^2, on different days of monolayer growth. Scale bar: 100 μm. C) Average Z projections of confocal microscopy images showing immunofluorescence (IF) staining for tight and adherens junction proteins ZO-1 and VE-cadherin on Day 6 of monolayer growth. Scale bar: 20 μm. D) Transport of FITC-dextran (FD) tracers across the monolayer after 4 h, on different days of monolayer growth. Data are shown as mean ± SD, n = 3.

2D). These values are consistent with other values reported in literature for *in vitro* BBB models and demonstrate that the monolayer possesses high structural integrity and selective permeability.[37,38] We also assessed the transendothelial electrical resistance (TEER) values of monolayers grown with our optimized cell seeding density, albeit in a 12-well transwell due to voltohmmeter electrode-plate compatibility. The TEER was around 20 Ω/cm^2 on Day 6 after cell seeding, consistent with other reported values (Figure S3).[37,38]

Going forward, prior to every LNP screening experiment done in HTS-BBB, we confirmed monolayer confluence using live/dead imaging as an easy, rapid, and low-resource method. Taken together, we optimized the growth of a brain endothelial monolayer on a 96-well transwell plate and demonstrated recapitulation of physiological properties of the BBB.

OPTIMIZING MRNA LNP TRANSFECTION AND TRANSPORT REPORTERS IN HTS-BBB

In order to use HTS-BBB for dual screening for both transfection of and transport across the BBB, LNPs needed to be loaded with reporters for both of these processes simultaneously without affecting transfection efficacy. Thus, we next optimized both the transfection and transport reporters and their readout conditions using LNPs made with C12-200, a gold standard ionizable lipid (Figure 3A).[39] LNPs were formulated with luciferase or mCherry mRNA and varying molar percentages of DiR, a fluorescent lipophilic dye for tracking transport across endothelial monolayers. All formulations were approximately 100 nm in size, with slight differences in polydispersity and similar mRNA encapsulation efficiencies of around 90% (Figure 3B).

We initially hypothesized that mCherry mRNA might be the preferred reporter since its readout is easily obtained by measuring fluorescence on a plate reader, whereas for luciferase mRNA, a luciferase assay must be performed prior to reading luminescence. This assay involves lysing cells and adding a substrate for the luciferase enzyme to react with and create bioluminescence. mCherry expression could also be visualized through fluorescence microscopy (Figure 3C). However, after assessing the fold change in signal over untreated cells for both mRNAs in a traditional 96-well plate, luminescence had a much more sensitive readout (Figure 3D). Interestingly, there was also an effect from the amount of DiR added, indicating that higher amounts of DiR may lower LNP transfection ability. Finally, there was a higher signal after 24 h of treatment

https://doi.org/10.1021/acs.nanolett.3c03509
Nano Lett. XXXX, XXX, XXX−XXX

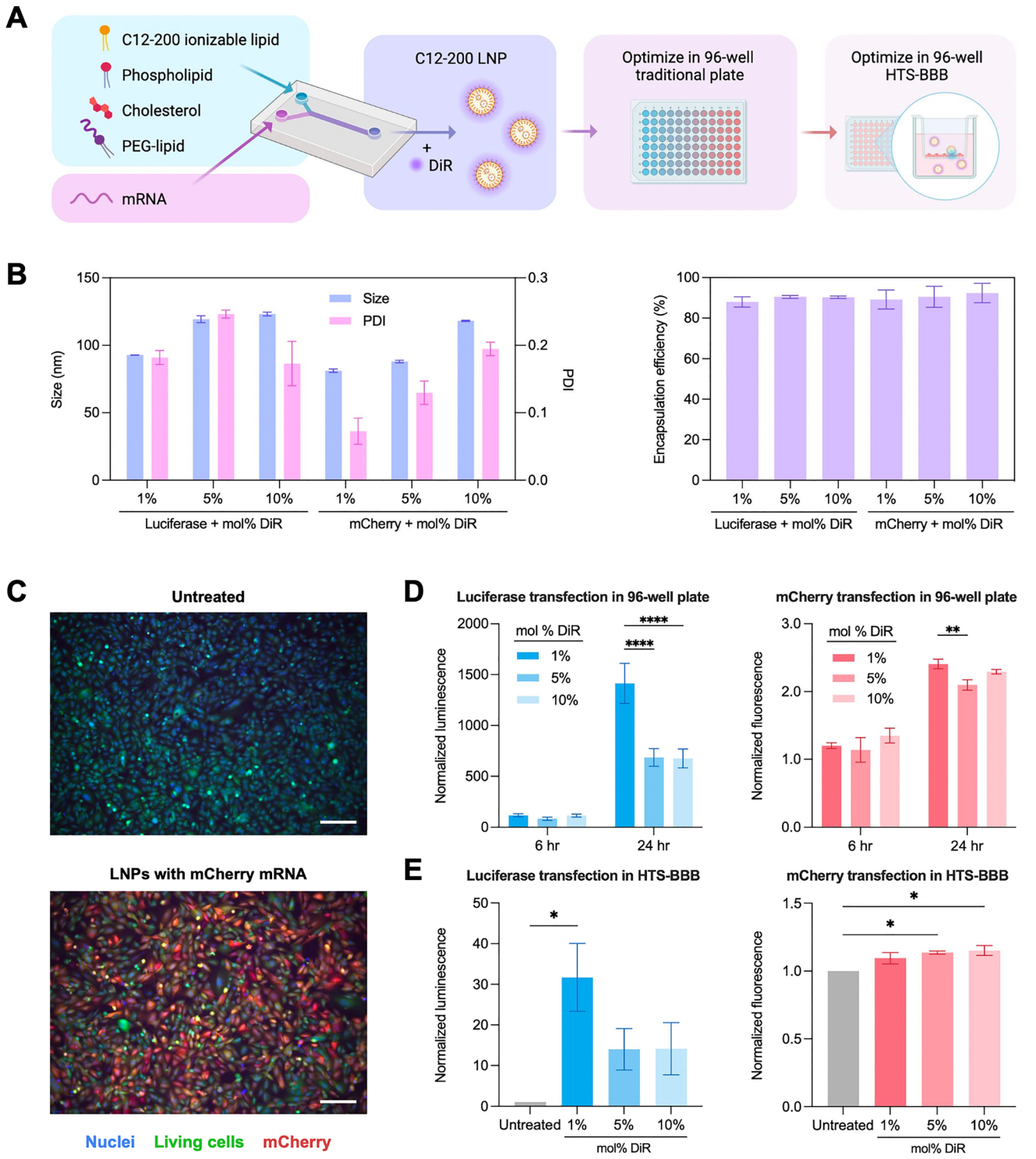

Figure 3. Optimization of mRNA LNP transfection and transport reporters in HTS-BBB. A) Schematic showing optimization process for transfection and transport readouts. B) Physicochemical characterization of C12-200 LNPs with varying reporter mRNAs and DiR molar percentages. Size and PDI is shown as mean ± SD, $n = 3$. Encapsulation efficiency is shown as mean ± SD, $n = 2$. C) mCherry expression in brain endothelial cells grown in a 96-well plate. Scale bar: 100 μm. D) Effect of DiR molar percentage on luciferase and mCherry expression in brain endothelial cells over time, in a 96-well plate. Cells were treated with 60 ng mRNA/20k cells. Data are shown as mean ± SD, $n = 3$, and normalized to untreated cells. Two-way ANOVA with Tukey's multiple comparisons test was used to determine statistical significance, $^{**}p < 0.01$, $^{****}p < 0.0001$. E) Effect of DiR molar percentage on luciferase and mCherry expression in brain endothelial cells, grown in HTS-BBB. Cells were treated with 60 ng mRNA/20k cells for 24 h. Data are shown as mean ± SD, $n = 3$, and normalized to untreated cells. One-way ANOVA with Tukey's multiple comparisons test was used to determine statistical significance, $^{*}p < 0.05$.

compared to 6 h, indicating that a longer treatment period allows for greater mRNA translation.

Given these results, the same LNPs were next tested in the HTS-BBB platform after 24 h of treatment (Figure 3E). By

https://doi.org/10.1021/acs.nanolett.3c03509
Nano Lett. XXXX, XXX, XXX−XXX

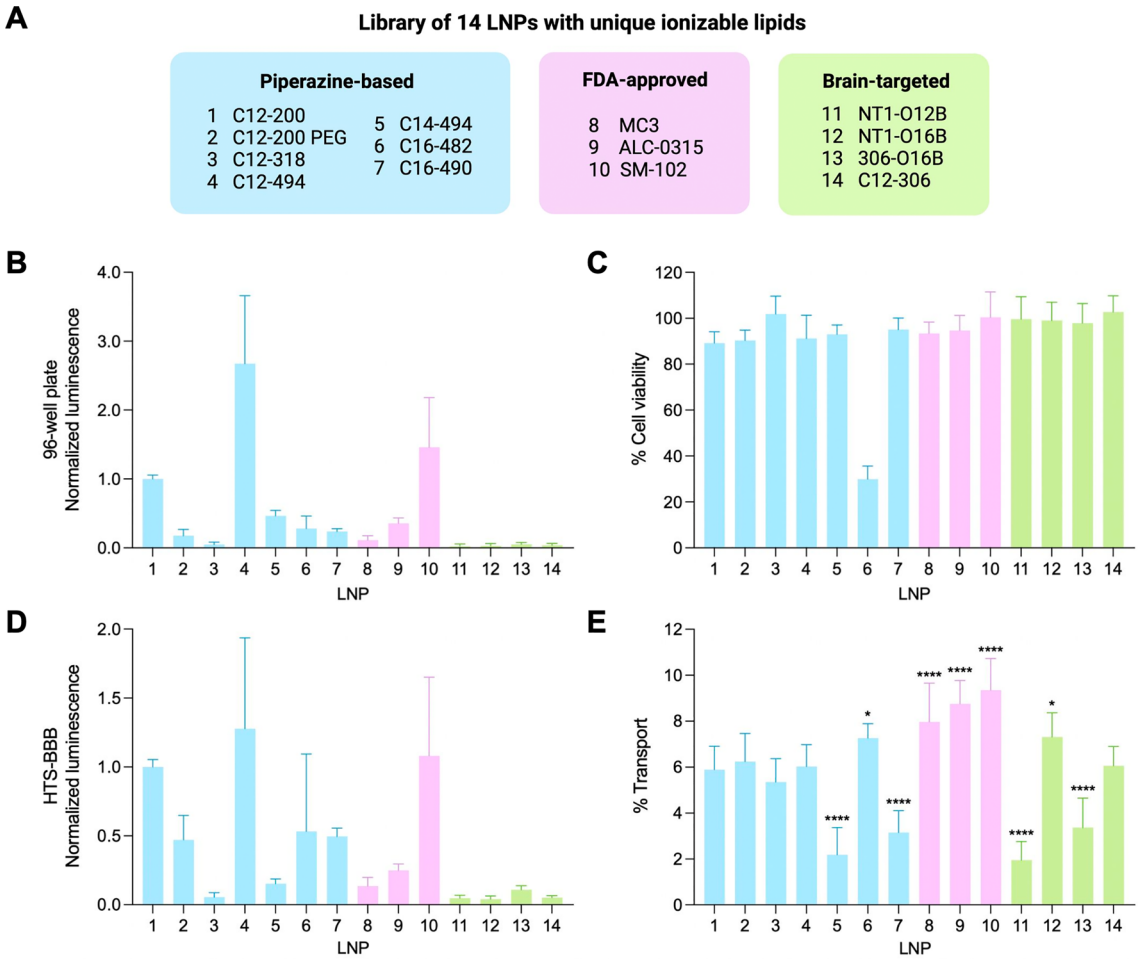

Figure 4. Screening of an LNP library in HTS-BBB for transfection and transport. A) Schematic showing design of library of 14 LNPs, each with a unique ionizable lipid. "C12-200 PEG" indicates a formulation with C12-200 as the ionizable lipid and a higher molar percentage of PEG-lipid. B) Luciferase expression in brain endothelial cells grown in a 96-well plate, treated with LNPs for 24 h at 60 ng mRNA/20k cells. Data are shown as mean + SD, $n = 3$ biological replicates each with $n = 3$ technical replicates, normalized to the C12-200 group. C) Cell viability of brain endothelial cells grown in a 96-well plate, treated with LNPs for 24 h at 60 ng mRNA/20k cells. Data are shown as mean + SD, $n = 3$ biological replicates each with $n = 3$ technical replicates, normalized to the untreated group. D) Luciferase expression in the brain endothelial monolayer of HTS-BBB, treated with LNPs for 24 h at 60 ng mRNA/20k cells. Data are shown as mean + SD, $n = 3$ biological replicates each with $n = 4$ technical replicates, normalized to the C12-200 group. E) Transport of LNPs across the brain endothelial monolayer of HTS-BBB after 24 h, as measured by DiR fluorescence from the LNPs. Data are shown as mean + SD, $n = 3$ biological replicates each with $n = 4$ technical replicates. One-way ANOVA with Dunnett's multiple comparisons test was used to determine statistical significance compared to the C12-200 group, $*p < 0.05$, $****p < 0.0001$.

creating a custom plate setting on the plate reader, we were able to accommodate the dimensions of the transwell plate which are slightly different from traditional 96-well plates. Once again, the luminescent readout was much more sensitive than the mCherry fluorescence readout, and the amount of DiR affected the luminescent signal. Thus, going forward luciferase mRNA and 1 mol % DiR were used for all LNP formulations, since it had the largest fold change in signal over untreated cells.

We also assessed additional strategies to quantify the transport of mRNA LNP across endothelial monolayers. First, we found that adding the surfactant Triton X-100 to the media prior to taking fluorescence readings increased DiR signal, likely by disrupting the LNPs (Figure S4). Thus, for all future HTS-BBB experiments, Triton X-100 was added to the media prior to taking readings. Second, we wanted to ensure that LNPs that crossed the monolayer were still intact and, thus, capable of transfecting other cells. To this end, dynamic light scattering (DLS) was first used to detect intact LNPs. While DLS was able to detect LNPs up to a 20-fold dilution in PBS, it was unable to detect LNPs at a 20-fold dilution in media (Figure S5A). We hypothesized that this might be due to the presence of serum proteins in the media, which could bind to LNPs and contribute to aggregation. To test this, LNPs were added to basolateral media, followed sequentially by nonprotein supplements, growth factors, and fetal bovine serum (FBS) to form the fully supplemented media, and then DLS readings were performed (Figure S5B). Indeed, the PDI of LNPs was significantly different from the PBS group after the addition of FBS, pointing toward serum interference. As an alternative approach, additional hCMEC/D3 cells were seeded in the basolateral compartment to see if they could be transfected by the mRNA LNPs. Indeed, there was transfection, indicating that LNPs which crossed the monolayer were intact and potent (Figure S6).

Thus, we were able to optimize parameters for measuring mRNA LNP transfection of and transport across an endothelial monolayer in a transwell system. We also showed that LNPs

https://doi.org/10.1021/acs.nanolett.3c03509
Nano Lett. XXXX, XXX, XXX−XXX

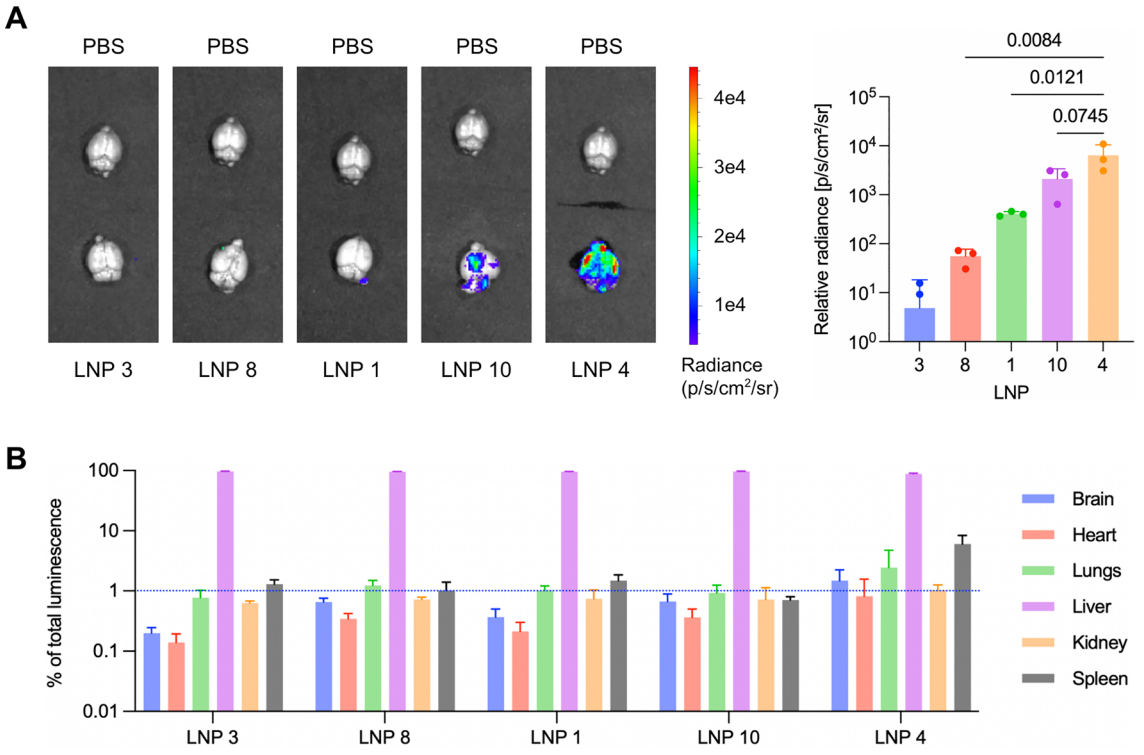

Figure 5. *In vivo* validation of the HTS-BBB mRNA LNP library screen. A) IVIS images and quantification of luciferase mRNA LNP delivery to the brain in adult C57BL/6 mice. Mice were injected intravenously with mRNA LNPs at a dose of 0.3 mg/kg mRNA or PBS and sacrificed after 6 h. Representative IVIS images are shown from the mouse dissected last per treatment group. Relative radiance was calculated by subtracting PBS luminescence from treated groups and reported as mean + SD with $n = 3$ biological replicates. One-way ANOVA with Šídák's multiple comparisons test was used to determine statistical significance. B) Distribution of luminescence across brain, heart, lungs, liver, kidneys, and spleen. Data are shown as % of total luminescence = (organ luminscence)/(total organ luminescnce) × 100. Blue dotted line indicates 1% of total organ delivery.

that crossed the monolayer retained their ability to transfect cells.

SCREENING A LIBRARY OF LNPS WITH UNIQUE IONIZABLE LIPIDS IN HTS-BBB

Having finished the optimization of HTS-BBB, we next evaluated whether this platform could detect transfection and transport differences between LNP formulations. To this end, a library of 14 LNPs with structurally diverse ionizable lipids was designed, each with luciferase mRNA and 1 mol % DiR (Figure 4A, Figure S7). LNPs 1 through 7 have ionizable lipids made with previously published piperazine-based cores and epoxide-terminated alkyl chains.[18,40−42] LNPs 8 through 10 have ionizable lipids that were used in FDA-approved formulations: MC3 which is used in the Onpattro LNP formulation, ALC-0315 which is used in the Pfizer-BioNTech COVID-19 vaccine, and SM-102 which is used in the Moderna COVID-19 vaccine.[43] LNPs 11 through 13 have ionizable lipids which were previously used in brain-targeted LNP formulations,[15,29] and LNP 14 has an ionizable lipid structurally similar to LNP 13 due to the 306 lipid core and was included in the same group for comparison.[44]

After characterizing the physicochemical properties of the library and measuring their mRNA encapsulation efficiencies, (Figure S8), LNP transfection and cytotoxicity was assessed in hCMEC/D3 cells grown in 96-well plates (Figure 4B,C). The library was then screened in HTS-BBB for monolayer transfection and transport (Figure 4D,E). While the LNPs exhibited similar transfection in hCMEC/D3 cells whether grown in a 96-well plate or HTS-BBB, they differed in transport across the endothelial monolayer in HTS-BBB. These statistically significant differences in transport confirmed that our model can robustly identify lead LNPs for transport across the monolayer.

Furthermore, LNPs 11 and 12 which have neurotransmitter-derived ionizable lipids had low brain endothelial transfection, which was expected since they were designed by Ma et al. to cross the BBB via active transport.[29] LNP 13 which has ionizable lipid 306-O16B was used to target glioblastoma cells by Liu et al.,[15] so its poor transfection of brain endothelial cells was also expected as it allows more to transport across the BBB rather than get trapped in the BBB.

Next, we assessed whether other LNP parameters correlated with transport across the monolayer. Transfection of the monolayer did not correlate with transport performance, indicating that screening in a model where both readouts are measured is critical (Figure S9). This implies that nanoparticle screening studies using endothelial cell uptake as a proxy for complete crossing of the BBB may not be entirely accurate. We next examined whether physical characteristics of the LNPs correlated with transport performance since there has been extensive prior research examining the effect of nanoparticle size on transport. Examples include studying polystyrene and protein-based nanoparticles,[37] gold nanoparticles,[45] and PEG−PLGA nanoparticles.[46] Size and zeta potential of the LNPs did not correlate with transport performance, potentially indicating that other LNP properties such as lipid structures may play a bigger role in transport (Figure S10). This agrees with the conclusion made by Ma et al. that differences in LNP brain delivery are likely a result of chemical properties rather than

https://doi.org/10.1021/acs.nanolett.3c03509
Nano Lett. XXXX, XXX, XXX−XXX

physical properties.[29] How these observations hold across nanoparticles made with different materials remains to be further studied.

Finally, we wanted to demonstrate that HTS-BBB could expand to include other cell types of interest. We conducted a proof-of-concept co-culture study with a brain endothelial monolayer grown on the transwell insert and differentiated neurons grown in the basolateral compartment. A portion of the LNP library was screened for three readouts: transport across the monolayer, transfection of the monolayer, and transfection of neurons (Figure S11). While in the monoculture screen LNPs 1, 4, and 10 were the best performing in endothelial transfection (Figure 4D), in the co-culture screen LNP 10 appeared as the distinct best performer (Figure S11B). Additionally, the selected piperazine-based LNPs had higher neuronal transfection than the FDA-approved LNPs and the selected brain-targeted LNP (Figure S11C). Future work may entail further optimization of media conditions for growth of both cell types as well as incorporating additional cell types of the neurovascular unit.

IN VIVO VALIDATION OF HTS-BBB LNP LIBRARY SCREEN

To confirm whether HTS-BBB was predictive of *in vivo* performance, we selected five lead LNPs from our *in vitro* screen to study biodistribution after systemic administration. We selected LNPs 3 and 8 because they have high transport and low monolayer transfection, and LNPs 1, 4, and 10 because they have high monolayer transfection. After formulating these LNPs with luciferase mRNA, healthy adult C57BL/6 mice were injected intravenously with PBS or LNPs at a dose of 0.3 mg/kg mRNA. After 6 h, mice were injected with luciferin to generate bioluminescent signal. Mice were then subjected to whole-body imaging to capture *in vivo* luminescent signal in the brain using an *in vivo* imaging system (IVIS) (Figure S12) or euthanized for organ collection, IVIS imaging, and quantification (Figure S13).

LNPs 4 and 10 demonstrated the greatest signal in the brain, with LNP 4 having about 1,000-fold greater signal than the bottom performer LNP 3 (Figure 5A). We then compared the luminescent signal that each organ contributed to the total organ luminescence and found that for LNP 4, the brain contributed approximately 1% of the signal, whereas for LNP 3 the brain only contributed approximately 0.2% (Figure 5B). LNP 4, with ionizable lipid C12-494, was previously shown to transfect endothelial cells in the placenta after intravenous injection, as well as induce vasodilation in the placenta after VEGF mRNA delivery.[40] It is possible that this LNP is able to transfect endothelial cells broadly since it appears to be well-suited toward extra-hepatic delivery, as shown in Figure 5B where compared to other LNPs there is more signal across all nonliver organs including the heart, lungs, kidney, and spleen. Future work should include investigation into whether certain chemical properties of C12-494 induce brain tropism, as well as which specific cell types in the neurovascular unit LNP 4 is able to transfect after systemic administration.

Even though LNP 3 had poor *in vivo* brain transfection, based on its excellent *in vitro* transport ability, we hypothesized that it may be transporting into the brain but not transfecting cells. This would support our earlier observation that transfection of and transport across endothelial cells are distinct. To test this, we conducted another biodistribution study with LNPs 3 and 4, formulated with 1 mol % DiR to track transport into the brain and mCherry mRNA to assess transfection. Healthy adult C57BL/6 mice were injected intravenously with PBS or LNPs at a dose of 0.5 mg/kg mRNA and sacrificed 24 h later. Both LNPs had greater DiR signal in the brain than the PBS group, indicating that both LNPs did indeed transport into the brain, and the difference between the two LNPs was not statistically significant (Figure S14A). LNP 4 had significantly greater mCherry signal than the PBS group, whereas LNP 3 did not (Figure S14B), which agreed with our first *in vivo* study using luciferase mRNA. Taken together, these data indicate that LNP delivery to the brain does not necessarily indicate transfection, and thus brain-targeted LNPs should be designed to have both targeting ability and brain transfection efficiency.

Finally, we further investigated the transfection and cellular uptake kinetics of our lead LNPs *in vitro*. We treated brain endothelial cells with LNPs containing luciferase mRNA and 1 mol % DiR, and measured luciferase transfection and DiR signal in cells at 1, 6, 24, 48, and 72 h. Luminescent signal peaked at 24 h across all LNP formulations (Figure S15A), further supporting what we observed in Figure 3D. DiR fluorescence peaked at 48 h across all formulations (Figure S15B), perhaps indicating that post-24 h, additional LNPs were able to enter cells, but mRNA may have begun degrading. It is worth noting that *in vitro* and *in vivo* kinetics likely vary due to the presence of additional physical forces and biological phenomena present *in vivo*. For instance, Pardi et al. found that after intravenous injection of luciferase mRNA LNPs, the highest measured luminescence was at 0.2 days.[47]

Overall, we have demonstrated that HTS-BBB can screen libraries of mRNA LNPs to identify formulations with either high transfection of brain endothelial cells or high transport across the brain endothelial monolayer and that the performance of lead candidates *in vitro* is recapitulated *in vivo*. This reinforces the case to use HTS-BBB to guide and increase the throughput of the development of brain-targeted LNPs for eventual treatment of neurological disorders.

In conclusion, we have developed HTS-BBB, a high-throughput *in vitro* screening platform for dual screening of mRNA LNP transfection of and transport across the BBB and demonstrated that it can predict *in vivo* delivery to the brain. Importantly, LNPs found to have high transfection and LNPs found to have high transport could both be used to treat neurological disorders. LNPs with high brain endothelial transfection may be used to deliver mRNA to aid in repairing the BBB, for example, in inflammatory brain pathologies including stroke and traumatic brain injury.[34] LNPs with high transport across the BBB may be further optimized to transfect specific brain cell types of interest, such as neurons or astrocytes. One limitation of HTS-BBB is its relative simplicity, with only endothelial cells and proof-of-concept co-culture with neurons. Future work may entail increasing the complexity of the platform to suit more tailored applications, such as by adding other cell types of interest like astrocytes, pericytes, or microglia, or by incorporating components to study neuroimmune communication.[48]

This platform would be ideal for screening large libraries of LNPs with brain-targeted peptides, antibodies, ionizable lipids, or varying molar ratios of lipid components to ultimately identify formulations with promise for treating neurological disorders. Optimized brain-targeted LNPs may also subsequently be used to deliver cargo beyond mRNAs, such as siRNAs, ASOs, DNAs, proteins, or small molecule drugs.

https://doi.org/10.1021/acs.nanolett.3c03509
Nano Lett. XXXX, XXX, XXX−XXX

Furthermore, the platform could be re-engineered for studying LNP delivery to and across other biological barriers such as the blood–placental barrier, to study pregnancy-related diseases, and the blood–retinal barrier, to study retinal diseases.

■ ASSOCIATED CONTENT

Supporting Information

The Supporting Information is available free of charge at https://pubs.acs.org/doi/10.1021/acs.nanolett.3c03509.

Materials and methods; figures showing monolayer growth optimization, monolayer characterization, transfection and transport reporter optimization, ionizable lipid structures, LNP library characterization, correlations from HTS-BBB screen, results from co-culture screen, in vivo whole-body imaging of lead LNP formulation, IVIS organ images, and in vitro kinetics of mRNA LNP transfection and uptake; table showing formulation details for LNP library (PDF)

■ AUTHOR INFORMATION

Corresponding Author

Michael J. Mitchell − *Department of Bioengineering, Institute for Immunology, Perelman School of Medicine, Cardiovascular Institute, Perelman School of Medicine, Institute for Regenerative Medicine, Perelman School of Medicine, Abramson Cancer Center, Perelman School of Medicine, and Penn Institute for RNA Innovation, Perelman School of Medicine, University of Pennsylvania, Philadelphia, Pennsylvania 19104, United States;* orcid.org/0000-0002-3628-2244; Email: mjmitch@seas.upenn.edu

Authors

Emily L. Han − *Department of Bioengineering, University of Pennsylvania, Philadelphia, Pennsylvania 19104, United States*

Marshall S. Padilla − *Department of Bioengineering, University of Pennsylvania, Philadelphia, Pennsylvania 19104, United States;* orcid.org/0000-0003-3607-790X

Rohan Palanki − *Department of Bioengineering, University of Pennsylvania, Philadelphia, Pennsylvania 19104, United States; Center for Fetal Research, Children's Hospital of Philadelphia, Philadelphia, Pennsylvania 19104, United States;* orcid.org/0000-0001-5168-5634

Dongyoon Kim − *Department of Bioengineering, University of Pennsylvania, Philadelphia, Pennsylvania 19104, United States*

Kaitlin Mrksich − *Department of Bioengineering, University of Pennsylvania, Philadelphia, Pennsylvania 19104, United States*

Jacqueline J. Li − *Department of Bioengineering, University of Pennsylvania, Philadelphia, Pennsylvania 19104, United States;* orcid.org/0000-0002-7849-5483

Sophia Tang − *Department of Bioengineering, University of Pennsylvania, Philadelphia, Pennsylvania 19104, United States*

Il-Chul Yoon − *Department of Bioengineering, University of Pennsylvania, Philadelphia, Pennsylvania 19104, United States*

Complete contact information is available at: https://pubs.acs.org/10.1021/acs.nanolett.3c03509

Author Contributions

E.L.H. and M.J.M. conceived the project and designed the experiments. The experiments were performed by E.L.H., M.S.P., R.P., D.K., K.M., J.J.L., S.T., and I.-C.Y. and interpreted by all authors. E.L.H. and M.J.M. wrote the manuscript, and E.L.H. and M.S.P. prepared the figures. All authors edited the manuscript and figures and approved the final version for submission.

Funding

M.J.M. acknowledges support from a US National Institutes of Health (NIH) Director's New Innovator Award (DP2 TR002776), a Burroughs Wellcome Fund Career Award at the Scientific Interface (CASI), a US National Science Foundation CAREER Award (CBET-2145491), and an American Cancer Society Research Scholar Grant (RSG-22-122-01-ET). E.L.H. acknowledges support from an NSF Graduate Research Fellowship (Award 1845298). M.S.P. acknowledges support from the National Institute of Dental and Craniofacial Research of the NIH (T90DE030854). R.P. acknowledges support from an NIH NHLBI F30 fellowship (F30HL162465-01A1).

Notes

The authors declare no competing financial interest.

■ ACKNOWLEDGMENTS

We thank the University of Pennsylvania's CDB Microscopy Core for the maintenance of the confocal microscope. We also thank Sai Chaluvadi and Bilal Elfayoumi for help with microscopy and Ryann Joseph for help with synthesis. Figure schematics were created with BioRender.

■ REFERENCES

(1) Feigin, V. L.; Vos, T.; Nichols, E.; Owolabi, M. O.; Carroll, W. M.; Dichgans, M.; Deuschl, G.; Parmar, P.; Brainin, M.; Murray, C. The Global Burden of Neurological Disorders: Translating Evidence into Policy. *Lancet Neurol.* **2020**, *19* (3), 255−265.

(2) Lu, Z.-G.; Shen, J.; Yang, J.; Wang, J.-W.; Zhao, R.-C.; Zhang, T.-L.; Guo, J.; Zhang, X. Nucleic Acid Drug Vectors for Diagnosis and Treatment of Brain Diseases. *Signal Transduct. Target. Ther.* **2023**, *8* (1), 1−53.

(3) Liu, C.; Shi, Q.; Huang, X.; Koo, S.; Kong, N.; Tao, W. mRNA-Based Cancer Therapeutics. *Nat. Rev. Cancer* **2023**, *23* (8), 526−543.

(4) Kim, M.; Oh, J.; Lee, Y.; Lee, E.-H.; Ko, S. H.; Jeong, J. H.; Park, C. H.; Lee, M. Delivery of Self-Replicating Messenger RNA into the Brain for the Treatment of Ischemic Stroke. *J. Controlled Release* **2022**, *350*, 471−485.

(5) Li, H.; Cao, Y.; Ye, J.; Yang, Z.; Chen, Q.; Liu, X.; Zhang, B.; Qiao, J.; Tang, Q.; Yang, H.; Li, J.; Shi, Z.; Mao, Y. Engineering Brain-Derived Neurotrophic Factor mRNA Delivery for the Treatment of Alzheimer's Disease. *Chem. Eng. J.* **2023**, *466*, No. 143152.

(6) Wang, P.; Zheng, X.; Guo, Q.; Yang, P.; Pang, X.; Qian, K.; Lu, W.; Zhang, Q.; Jiang, X. Systemic Delivery of BACE1 siRNA through Neuron-Targeted Nanocomplexes for Treatment of Alzheimer's Disease. *J. Controlled Release* **2018**, *279*, 220−233.

(7) Yang, X.; Yang, W.; Xia, X.; Lei, T.; Yang, Z.; Jia, W.; Zhou, Y.; Cheng, G.; Gao, H. Intranasal Delivery of BACE1 siRNA and Rapamycin by Dual Targets Modified Nanoparticles for Alzheimer's Disease Therapy. *Small* **2022**, *18* (30), 2203182.

(8) Shyam, R.; Ren, Y.; Lee, J.; Braunstein, K. E.; Mao, H.-Q.; Wong, P. C. Intraventricular Delivery of siRNA Nanoparticles to the Central Nervous System. *Mol. Ther. - Nucleic Acids* **2015**, *4*, No. e242.

(9) Zhou, Y.; Zhu, F.; Liu, Y.; Zheng, M.; Wang, Y.; Zhang, D.; Anraku, Y.; Zou, Y.; Li, J.; Wu, H.; Pang, X.; Tao, W.; Shimoni, O.; Bush, A. I.; Xue, X.; Shi, B. Blood-Brain Barrier−Penetrating siRNA

Nanomedicine for Alzheimer's Disease Therapy. *Sci. Adv.* **2020**, *6* (41), No. eabc7031.
(10) Park, T.-E.; Singh, B.; Li, H.; Lee, J.-Y.; Kang, S.-K.; Choi, Y.-J.; Cho, C.-S. Enhanced BBB Permeability of Osmotically Active Poly(Mannitol-Co-PEI) Modified with Rabies Virus Glycoprotein via Selective Stimulation of Caveolar Endocytosis for RNAi Therapeutics in Alzheimer's Disease. *Biomaterials* **2015**, *38*, 61−71.
(11) Zheng, X.; Pang, X.; Yang, P.; Wan, X.; Wei, Y.; Guo, Q.; Zhang, Q.; Jiang, X. A Hybrid siRNA Delivery Complex for Enhanced Brain Penetration and Precise Amyloid Plaque Targeting in Alzheimer's Disease Mice. *Acta Biomater.* **2017**, *49*, 388−401.
(12) Helmschrodt, C.; Höbel, S.; Schöniger, S.; Bauer, A.; Bonicelli, J.; Gringmuth, M.; Fietz, S. A.; Aigner, A.; Richter, A.; Richter, F. Polyethylenimine Nanoparticle-Mediated siRNA Delivery to Reduce α-Synuclein Expression in a Model of Parkinson's Disease. *Mol. Ther. - Nucleic Acids* **2017**, *9*, 57−68.
(13) Schlich, M.; Longhena, F.; Faustini, G.; O'Driscoll, C. M.; Sinico, C.; Fadda, A. M.; Bellucci, A.; Lai, F. Anionic Liposomes for Small Interfering Ribonucleic Acid (siRNA) Delivery to Primary Neuronal Cells: Evaluation of Alpha-Synuclein Knockdown Efficacy. *Nano Res.* **2017**, *10* (10), 3496−3508.
(14) Peng, H.; Guo, X.; He, J.; Duan, C.; Yang, M.; Zhang, X.; Zhang, L.; Fu, R.; Wang, B.; Wang, D.; Chen, H.; Xie, M.; Feng, P.; Dai, L.; Tang, X.; Luo, J. Intracranial Delivery of Synthetic mRNA to Suppress Glioblastoma. *Mol. Ther. - Oncolytics* **2022**, *24*, 160−170.
(15) Liu, S.; Liu, J.; Li, H.; Mao, K.; Wang, H.; Meng, X.; Wang, J.; Wu, C.; Chen, H.; Wang, X.; Cong, X.; Hou, Y.; Wang, Y.; Wang, M.; Yang, Y.-G.; Sun, T. An Optimized Ionizable Cationic Lipid for Brain Tumor-Targeted siRNA Delivery and Glioblastoma Immunotherapy. *Biomaterials* **2022**, *287*, No. 121645.
(16) Kozielski, K. L.; Ruiz-Valls, A.; Tzeng, S. Y.; Guerrero-Cázares, H.; Rui, Y.; Li, Y.; Vaughan, H. J.; Gionet-Gonzales, M.; Vantucci, C.; Kim, J.; Schiapparelli, P.; Al-Kharboosh, R.; Quiñones-Hmojosa, A.; Green, J. J. Cancer-Selective Nanoparticles for Combinatorial siRNA Delivery to Primary Human GBM in Vitro and in Vivo. *Biomaterials* **2019**, *209*, 79−87.
(17) Rosenblum, D.; Gutkin, A.; Kedmi, R.; Ramishetti, S.; Veiga, N.; Jacobi, A. M.; Schubert, M. S.; Friedmann-Morvinski, D.; Cohen, Z. R.; Behlke, M. A.; Lieberman, J.; Peer, D. CRISPR-Cas9 Genome Editing Using Targeted Lipid Nanoparticles for Cancer Therapy. *Sci. Adv.* **2020**, *6* (47), No. eabc9450.
(18) Palanki, R.; Bose, S. K.; Dave, A.; White, B. M.; Berkowitz, C.; Luks, V.; Yaqoob, F.; Han, E.; Swingle, K. L.; Menon, P.; Hodgson, E.; Biswas, A.; Billingsley, M. M.; Li, L.; Yiping, F.; Carpenter, M.; Trokhan, A.; Yeo, J.; Johana, N.; Wan, T. Y.; Alameh, M.-G.; Bennett, F. C.; Storm, P. B.; Jain, R.; Chan, J.; Weissman, D.; Mitchell, M. J.; Peranteau, W. H. Ionizable Lipid Nanoparticles for Therapeutic Base Editing of Congenital Brain Disease. *ACS Nano* **2023**, *17* (14), 13594−13610.
(19) Huang, X.; Kong, N.; Zhang, X.; Cao, Y.; Langer, R.; Tao, W. The Landscape of mRNA Nanomedicine. *Nat. Med.* **2022**, *28* (11), 2273−2287.
(20) Hamilton, A. G.; Swingle, K. L.; Mitchell, M. J. Biotechnology: Overcoming Biological Barriers to Nucleic Acid Delivery Using Lipid Nanoparticles. *PLOS Biol.* **2023**, *21* (4), No. e3002105.
(21) Safford, H. C.; Swingle, K. L.; Geisler, H. C.; Hamilton, A. G.; Thatte, A. S.; Ghalsasi, A. A.; Billingsley, M. M.; Alameh, M.; Weissman, D.; Mitchell, M. J. Orthogonal Design of Experiments for Engineering of Lipid Nanoparticles for mRNA Delivery to the Placenta. *Small* **2023**, No. 2303568.
(22) Raguram, A.; Banskota, S.; Liu, D. R. Therapeutic in Vivo Delivery of Gene Editing Agents. *Cell* **2022**, *185* (15), 2806−2827.
(23) Cheng, Q.; Wei, T.; Farbiak, L.; Johnson, L. T.; Dilliard, S. A.; Siegwart, D. J. Selective Organ Targeting (SORT) Nanoparticles for Tissue-Specific mRNA Delivery and CRISPR−Cas Gene Editing. *Nat. Nanotechnol.* **2020**, *15* (4), 313−320.
(24) Kularatne, R. N.; Crist, R. M.; Stern, S. T. The Future of Tissue-Targeted Lipid Nanoparticle-Mediated Nucleic Acid Delivery. *Pharmaceuticals* **2022**, *15* (7), 897.
(25) Nakamura, T.; Sato, Y.; Yamada, Y.; Abd Elwakil, M. M.; Kimura, S.; Younis, M. A.; Harashima, H. Extrahepatic Targeting of Lipid Nanoparticles in Vivo with Intracellular Targeting for Future Nanomedicines. *Adv. Drug Delivery Rev.* **2022**, *188*, No. 114417.
(26) Pardridge, W. M. Blood-Brain Barrier and Delivery of Protein and Gene Therapeutics to Brain. *Front. Aging Neurosci.* **2020**, *11*, 00373.
(27) Khare, P.; Edgecomb, S. X.; Hamadani, C. M.; Tanner, E. E. L.; S Manickam, D. Lipid Nanoparticle-Mediated Drug Delivery to the Brain. *Adv. Drug Delivery Rev.* **2023**, *197*, No. 114861.
(28) Pardridge, W. M. The Blood-Brain Barrier: Bottleneck in Brain Drug Development. *NeuroRX* **2005**, *2* (1), 3−14.
(29) Ma, F.; Yang, L.; Sun, Z.; Chen, J.; Rui, X.; Glass, Z.; Xu, Q. Neurotransmitter-Derived Lipidoids (NT-Lipidoids) for Enhanced Brain Delivery through Intravenous Injection. *Sci. Adv.* **2020**, *6* (30), No. eabb4429.
(30) Shah, B.; Dong, X. Current Status of In Vitro Models of the Blood-Brain Barrier. *Curr. Drug Delivery* **2022**, *19*, 1034−1046.
(31) Stone, N. L.; England, T. J.; O'Sullivan, S. E. A Novel Transwell Blood Brain Barrier Model Using Primary Human Cells. *Front. Cell. Neurosci.* **2019**, *13*, 00230.
(32) D'Souza, A.; Dave, K. M.; Stetler, R. A.; S. Manickam, D. Targeting the Blood-Brain Barrier for the Delivery of Stroke Therapies. *Adv. Drug Delivery Rev.* **2021**, *171*, 332−351.
(33) Sweeney, M. D.; Zhao, Z.; Montagne, A.; Nelson, A. R.; Zlokovic, B. V. Blood-Brain Barrier: From Physiology to Disease and Back. *Physiol. Rev.* **2019**, *99* (1), 21−78.
(34) Marcos-Contreras, O. A.; Greineder, C. F.; Kiseleva, R. Y.; Parhiz, H.; Walsh, L. R.; Zuluaga-Ramirez, V.; Myerson, J. W.; Hood, E. D.; Villa, C. H.; Tombacz, I.; Pardi, N.; Seliga, A.; Mui, B. L.; Tam, Y. K.; Glassman, P. M.; Shuvaev, V. V.; Nong, J.; Brenner, J. S.; Khoshnejad, M.; Madden, T.; Weissmann, D.; Persidsky, Y.; Muzykantov, V. R. Selective Targeting of Nanomedicine to Inflamed Cerebral Vasculature to Enhance the Blood−Brain Barrier. *Proc. Natl. Acad. Sci. U. S. A.* **2020**, *117* (7), 3405−3414.
(35) Weksler, B.; Romero, I. A.; Couraud, P.-O. The hCMEC/D3 Cell Line as a Model of the Human Blood Brain Barrier. *Fluids Barriers CNS* **2013**, *10* (1), 16.
(36) Luissint, A.-C.; Artus, C.; Glacial, F.; Ganeshamoorthy, K.; Couraud, P.-O. Tight Junctions at the Blood Brain Barrier: Physiological Architecture and Disease-Associated Dysregulation. *Fluids Barriers CNS* **2012**, *9* (1), 23.
(37) Brown, T. D.; Habibi, N.; Wu, D.; Lahann, J.; Mitragotri, S. Effect of Nanoparticle Composition, Size, Shape, and Stiffness on Penetration Across the Blood−Brain Barrier. *ACS Biomater. Sci. Eng.* **2020**, *6* (9), 4916−4928.
(38) Sun, J.; Ou, W.; Han, D.; Paganini-Hill, A.; Fisher, M. J.; Sumbria, R. K. Comparative Studies between the Murine Immortalized Brain Endothelial Cell Line (bEnd.3) and Induced Pluripotent Stem Cell-Derived Human Brain Endothelial Cells for Paracellular Transport. *PLoS One* **2022**, *17* (5), No. e0268860.
(39) Han, X.; Zhang, H.; Butowska, K.; Swingle, K. L.; Alameh, M.-G.; Weissman, D.; Mitchell, M. J. An Ionizable Lipid Toolbox for RNA Delivery. *Nat. Commun.* **2021**, *12* (1), 7233.
(40) Swingle, K. L.; Safford, H. C.; Geisler, H. C.; Hamilton, A. G.; Thatte, A. S.; Billingsley, M. M.; Joseph, R. A.; Mrksich, K.; Padilla, M. S.; Ghalsasi, A. A.; Alameh, M.-G.; Weissman, D.; Mitchell, M. J. Ionizable Lipid Nanoparticles for *In Vivo* mRNA Delivery to the Placenta during Pregnancy. *J. Am. Chem. Soc.* **2023**, *145* (8), 4691−4706.
(41) Kim, M.; Jeong, M.; Hur, S.; Cho, Y.; Park, J.; Jung, H.; Seo, Y.; Woo, H. A.; Nam, K. T.; Lee, K.; Lee, H. Engineered Ionizable Lipid Nanoparticles for Targeted Delivery of RNA Therapeutics into Different Types of Cells in the Liver. *Sci. Adv.* **2021**, *7* (9), No. eabf4398.
(42) Billingsley, M. M.; Singh, N.; Ravikumar, P.; Zhang, R.; June, C. H.; Mitchell, M. J. Ionizable Lipid Nanoparticle-Mediated mRNA Delivery for Human CAR T Cell Engineering. *Nano Lett.* **2020**, *20* (3), 1578−1589.

https://doi.org/10.1021/acs.nanolett.3c03509
Nano Lett. XXXX, XXX, XXX−XXX

(43) Schoenmaker, L.; Witzigmann, D.; Kulkarni, J. A.; Verbeke, R.; Kersten, G.; Jiskoot, W.; Crommelin, D. J. A. mRNA-Lipid Nanoparticle COVID-19 Vaccines: Structure and Stability. *Int. J. Pharm.* **2021**, *601*, No. 120586.
(44) Whitehead, K. A.; Dorkin, J. R.; Vegas, A. J.; Chang, P. H.; Veiseh, O.; Matthews, J.; Fenton, O. S.; Zhang, Y.; Olejnik, K. T.; Yesilyurt, V.; Chen, D.; Barros, S.; Klebanov, B.; Novobrantseva, T.; Langer, R.; Anderson, D. G. Degradable Lipid Nanoparticles with Predictable in Vivo siRNA Delivery Activity. *Nat. Commun.* **2014**, *5* (1), 4277.
(45) Shilo, M.; Sharon, A.; Baranes, K.; Motiei, M.; Lellouche, J.-P. M.; Popovtzer, R. The Effect of Nanoparticle Size on the Probability to Cross the Blood-Brain Barrier: An in-Vitro Endothelial Cell Model. *J. Nanobiotechnology* **2015**, *13* (1), 19.
(46) Meng, Q.; Meng, H.; Pan, Y.; Liu, J.; Li, J.; Qi, Y.; Huang, Y. Influence of Nanoparticle Size on Blood−Brain Barrier Penetration and the Accumulation of Anti-Seizure Medicines in the Brain. *J. Mater. Chem. B* **2022**, *10* (2), 271−281.
(47) Pardi, N.; Tuyishime, S.; Muramatsu, H.; Kariko, K.; Mui, B. L.; Tam, Y. K.; Madden, T. D.; Hope, M. J.; Weissman, D. Expression Kinetics of Nucleoside-Modified mRNA Delivered in Lipid Nanoparticles to Mice by Various Routes. *J. Control. Release Off. J. Control. Release Soc.* **2015**, *217*, 345−351.
(48) Erickson, M. A.; Wilson, M. L.; Banks, W. A. In Vitro Modeling of Blood−Brain Barrier and Interface Functions in Neuroimmune Communication. *Fluids Barriers CNS* **2020**, *17* (1), 26.

https://doi.org/10.1021/acs.nanolett.3c03509
Nano Lett. XXXX, XXX, XXX−XXX